Electronic supplementary information

Efficient CO_2 conversion to CO using chemical looping over Co-In oxide

Jun-Ichiro Makiura, Sota Kakihara, Takuma Higo, Naoki Ito, Yuichiro Hirano and Yasushi Sekine*

*Correspondence to; Yasushi SEKINE: ysekine@waseda.jp

This file includes:

- Supplementary text
- Figures S1 to S7
- Tables S1 to S5

Supplementary text

Preparation of RWGS-CL materials

Co-In oxide (Co-In_2O_3) used in this study was prepared in two steps. In the first step, In_2O_3 was prepared by the complex polymerization method. $In(NO_3)_3 \cdot nH_2O$, excess amounts of ethylene glycol and citric acid were first dissolved in distilled water. Next, the solution was stirred for 18 hours in a water bath, which was set at 353 K. After that, the solution was dried on a hot stirrer and pre-calcined for 2 hours at 673 K. Finally, the obtained powder was calcined for 10 hours at 1123 K. In the second step, $Co(NO_3)_2 \cdot 6H_2O$ was impregnated into In_2O_3. First, In_2O_3 prepared in the first step was soaked in distilled water and stirred in a rotary evaporator *in vacuo* for 2 hours at room temperature. Secondly, Co nitrite was added to the solution, followed by stirring with the same method. The stirred solution was dried and heated in an oven at 393 K. Finally, the obtained powder was calcined for 5 hours at 773 K. Taking account of thermodynamically favorable ratio of Co-In alloy in the medium temperature range[28], the preparation molar ratio of Co and In was set to be 1:2.

Procedure of Isothermal RWGS-CL test

An isothermal RWGS-CL cycle test was performed using a thermogravimetric analyzer (TG-50A; Shimadzu Corp.). First, the 30 mg of sample powder filled in a sample pan was heated to the target temperature in an Ar atmosphere. The oxide powder was then reduced by 10 vol% H_2 balanced by Ar for 30 minutes (reduction step). After the reduction step, the reduced oxide was re-oxidized by 10 vol% CO_2 balanced by Ar until no increase in the sample weight was observed. This series of reduction and oxidation steps was defined as one cycle for the isothermal RWGS-CL. The total flow rate was set constant at 100 mL min^{-1}. The amount of reduction and oxidation (redox) was defined as the amount of oxygen atom released or backfilled in each step and was calculated from the weight change of the material during the reaction (For convenience, the endpoint of re-oxidation was defined as the point where the oxidation rate reached below 10 μmol min^{-1} g^{-1}).

The calculation formula for the amount redox is as follows;

$$\text{Amount of reduction or oxidation (redox) [mmol g}^{-1}\text{]} = \frac{|\Delta m|}{m_{\text{sample}} \times M_{\text{O}}} \qquad \text{(S1)}$$

where Δm / mg, m_{sample} / g and M_{O}/ g mol^{-1} represent weight change of the sample during the cycle test, the initial sample weight of the sample (regarding Co existing as a metallic state) and the molar mass of the oxygen atom respectively.

The calculation formula for the average CO_2 splitting rate is

$$\text{Average CO}_2 \text{ splitting rate } [\mu\text{mol g}^{-1} \text{ min}^{-1}] = \frac{\text{Amount of oxidation}}{\Delta t} \times 10^3 \tag{S2}$$

where Δt / min represents the time required for the re-oxidation.

Evaluation of maximum CO_2 conversion

The maximum CO_2 conversion of the oxidation reaction (Eq. 5) was evaluated using a thermogravimetric analyzer (TG-50A; Shimadzu Corp.). First, the sample was reduced by 10%H_2 balanced by Ar. After the reduction, CO-CO_2 mixed gas was introduced at a certain CO/CO_2 ratio. When an increase in the weight of the oxide sample was observed, it was considered that the oxidation reaction (Eq. 5) proceeded forward (left to right) at the CO/CO_2 ratio. For that case, CO-CO_2 mixed gas having a higher CO/CO_2 ratio was introduced. This series of operations was done until the weight of the oxide sample started to decrease, and the CO/CO_2 ratio just before the CO-CO_2 ratio at which the weight started to decrease was defined as the maximum CO_2 conversion of the sample.

Structural Characterization

Crystal structures of Co-In_2O_3 at various states were analyzed using an X-ray diffractometer (Smart Lab III; Rigaku Corp). The analysis was performed using Cu-$K\alpha$ radiation under the conditions of 40 kV and 40 mA. The morphology of the sample particle and the dispersion of the contained elements were observed using a scanning transmission electron microscope with an energy-dispersive X-ray spectrometer (STEM-EDX; HE-2200; Hitachi Ltd.). *In-situ* X-ray absorption fine structure (XAFS) measurements in transmission mode for In and Co *K*-edge were conducted at the beamline BL14B2 of the SPring-8. The beam size at the sample position was 1 (vertical) mm × 5.0 (horizontal) mm. High harmonic contamination of the beam was rejected by a pair of Rh-coated Si mirrors. The incident X-ray was monochromatized using a pair of Si(111) crystals. The Co-In_2O_3 powder diluted by boron nitride (BN) was pressed into a 10 mmϕ disk. The disk was attached to a cell for *in-situ* experiments. The sample was heated in N_2 flow, and alternatively exposed to 10% H_2 and 40% CO_2 in N_2 at 773 K. The spectra were recorded in each atmosphere at 773 K. The total flow rate was set constant to 100 mL min^{-1} in the experiments. The obtained spectra were analyzed using software (Athena ver. 0.9.26).

The details for the results of *in-situ* XAFS measurements

To investigate more details of the redox mechanism of Co-In_2O_3, *in-situ* XAFS measurements were conducted. XAFS results are shown in Figs 4(A)–(C). The spectra for Co-In_2O_3 catalyst gradually changed due to the exposure to 10%H_2 atmosphere (Fig. 4(A)). The intensity of white-line decreased over time, which indicates that In(III) in Co-In_2O_3 was reduced to In(0) by H_2. Using a linear combination fitting (LCF) analysis between the metallic state and the oxidized state of In, the reduction of In(III) in Co-In_2O_3 was estimated to proceed by 27.9 % in 60 min (Table S2). Then, the intensity of white-line increased during the exposure to 40%CO_2 due to re-oxidation of In(0). The sequential change of In *K*-edge spectra indicates that the redox of In(III) 👎 In(0) occurs during the RWGS-CL cycle. Fig. 4(C) shows spectra for Co *K*-edge of Co-In_2O_3 in 40%CO_2 atmosphere following the exposure to 10%H_2 for 60 min. After the exposure to 10%H_2, the spectra were similar to that of Co-foil, but showed slightly different features (blue line in Fig. 4(C)). These spectra cannot be replicated by a linear combination of the spectra of Co-foil and CoO as standard samples, which suggests the formation of Co-In alloy in addition to Co metal. When the reduced Co-In_2O_3 was exposed to CO_2, the absorption edge gradually shifted to the lower energy (red lines in Fig. 4(C)). The behavior represents the oxidative change of Co-In alloy to Co metal and In_2O_3.

Reaction kinetic models

In order to elucidate the mechanism of the isothermal RWGS-CL on Co-In_2O_3, the reaction kinetic study was conducted. The method[29] which was proposed by Hancock and Sharp can distinguish the reaction mechanisms. The following equation S3 derives from Avrami-Erofe'ev equation[32–34] which is based on the classical nucleation and grain growth model.

$$\ln\left(-\ln\left(1-x\right)\right)=\ln\left(a\right)+n\ln\left(t\right) \qquad \text{(S3)}$$

where x is the fraction reacted in time t (: the solid conversion), a is the constant based on the frequency of the nuclei formation and the rate of grain growth, and n is the constant associated with the geometry of the system.

In this method, a suitable model is inferred using the plots of ln(−ln(1−x) *vs.* ln(t). Table S3 shows rate equations and n values for typical reaction models for isothermal solid-phase reactions. Hancock and Sharp proposed that linear plots can be obtained for these models other than the nucleation and grain growth model as well, if the conversion x is limited to the range of 0.15–0.5. Therefore, the value of slope n obtained from the plots allows to verify the kinetic model, and this method has been employed in previous literature for the chemical-looping process[30, 31].

Model fitting for the oxidation of reduced Co-In_2O_3

In this study, the experimental data for the oxidation by CO_2 was obtained by a thermogravimetry. The conversion of Co-In_2O_3 in the oxidation step was defined as the following equation S4.

$$x(oxidation) = \frac{m_t - m_i}{m_f - m_i} \tag{S4}$$

where m_i is the initial weight (: the weight of Co-In_2O_3 after reduction by H_2), m_t is the weight at the time t and m_f is the final weight (: the weight of Co-In_2O_3 after completion of oxidation by CO_2). In this investigation, the reduction amount was adjusted to the range of 3.02–3.46 mmol g^{-1} at all temperatures. Fig S4 shows the plots of ln(−ln(1−x)) vs. ln(t) for the oxidation of the reduced Co-In_2O_3. The candidates for fittings were AE1, R1, R2 and R3 models since the average n values were 1.274–1.364. The experimental and calculated conversion are shown in Fig S5, and Table S4 shows values of root-mean square deviation (RMSD). As these results, the zero-order reaction model (R1) shows a good fitting for the conversion till ca. 70% (Fig S5 and Table S4).

RWGS-CL performance of Co-In based oxides with different preparation methods and Co/In ratios

In order to investigate more details about Co-In based oxides, experiments were carried out on Co-In based oxides with different Co/In ratios. The results are shown in Table S5. As a result, there was a tendency for the CO_2 splitting amount to increase and the average CO_2 splitting rate to decrease as the Co/In ratio increased. These tendencies may be due to the amount of Co-In alloy formed and the distribution of Co species on In_2O_3.

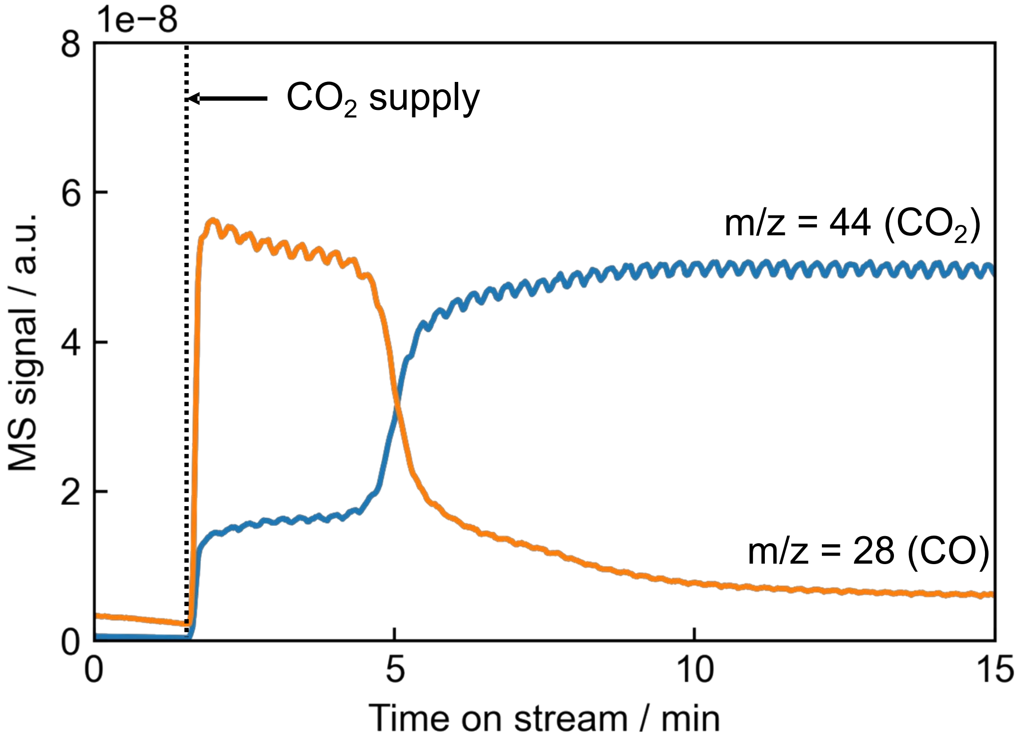

Fig. S1. CO formation during re-oxidation step on Co-In_2O_3 at 773 K.

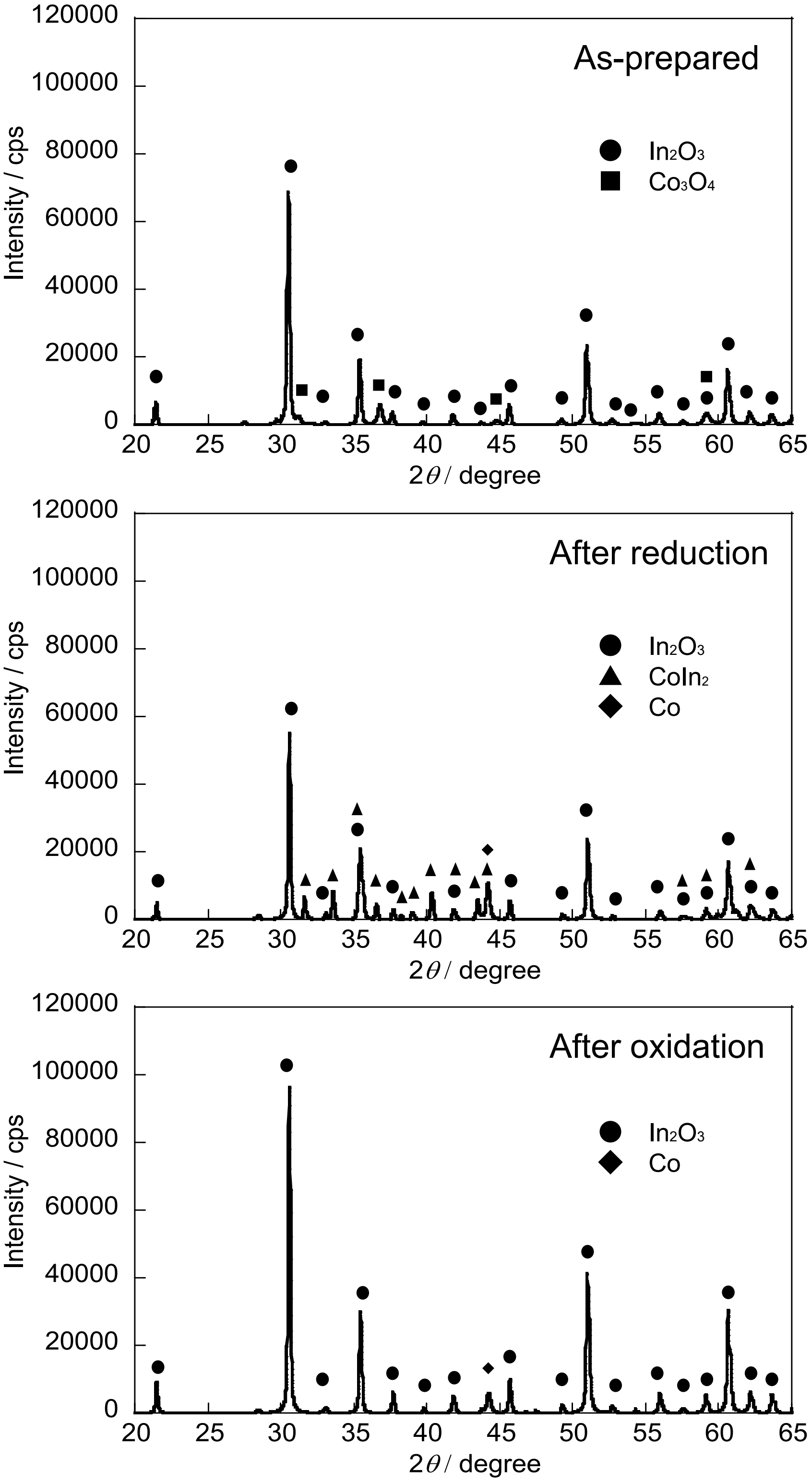

Fig. S2. XRD profile of Co-In_2O_3 during RWGS-CL.

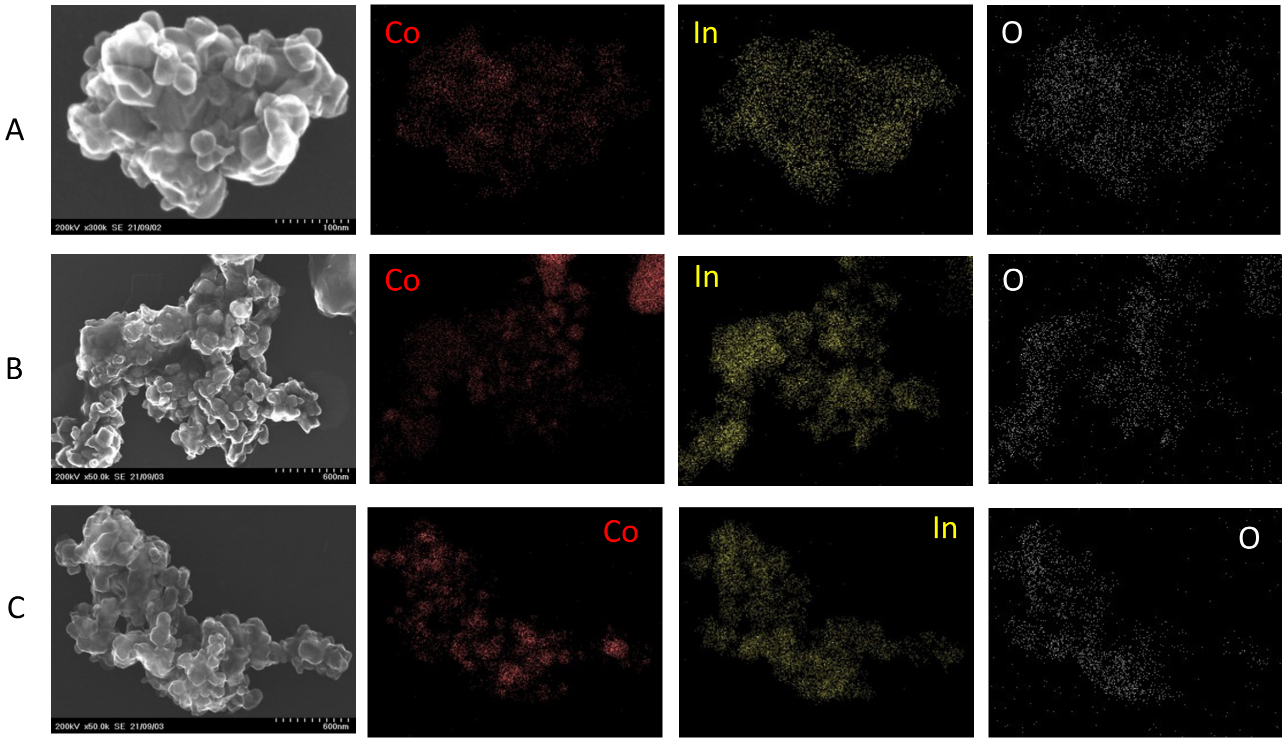

Fig. S3. STEM-EDX images of Co-In_2O_3 (A) as-prepared (B) after reduction and (C) after oxidation.

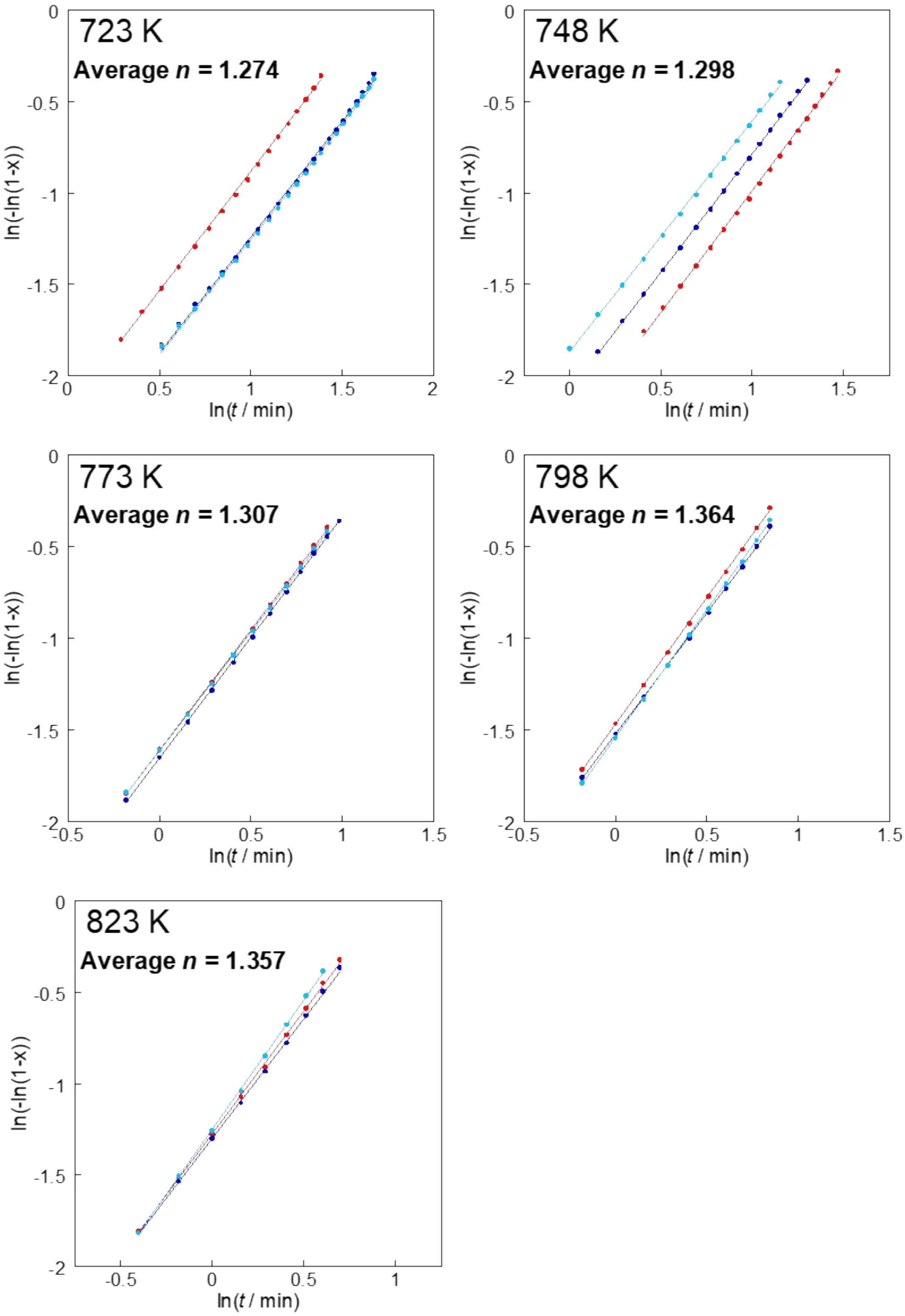

Fig. S4. Plots of ln(−ln(1−x)) *vs*. ln(t) for oxidation of the reduced Co-In_2O_3 by CO_2

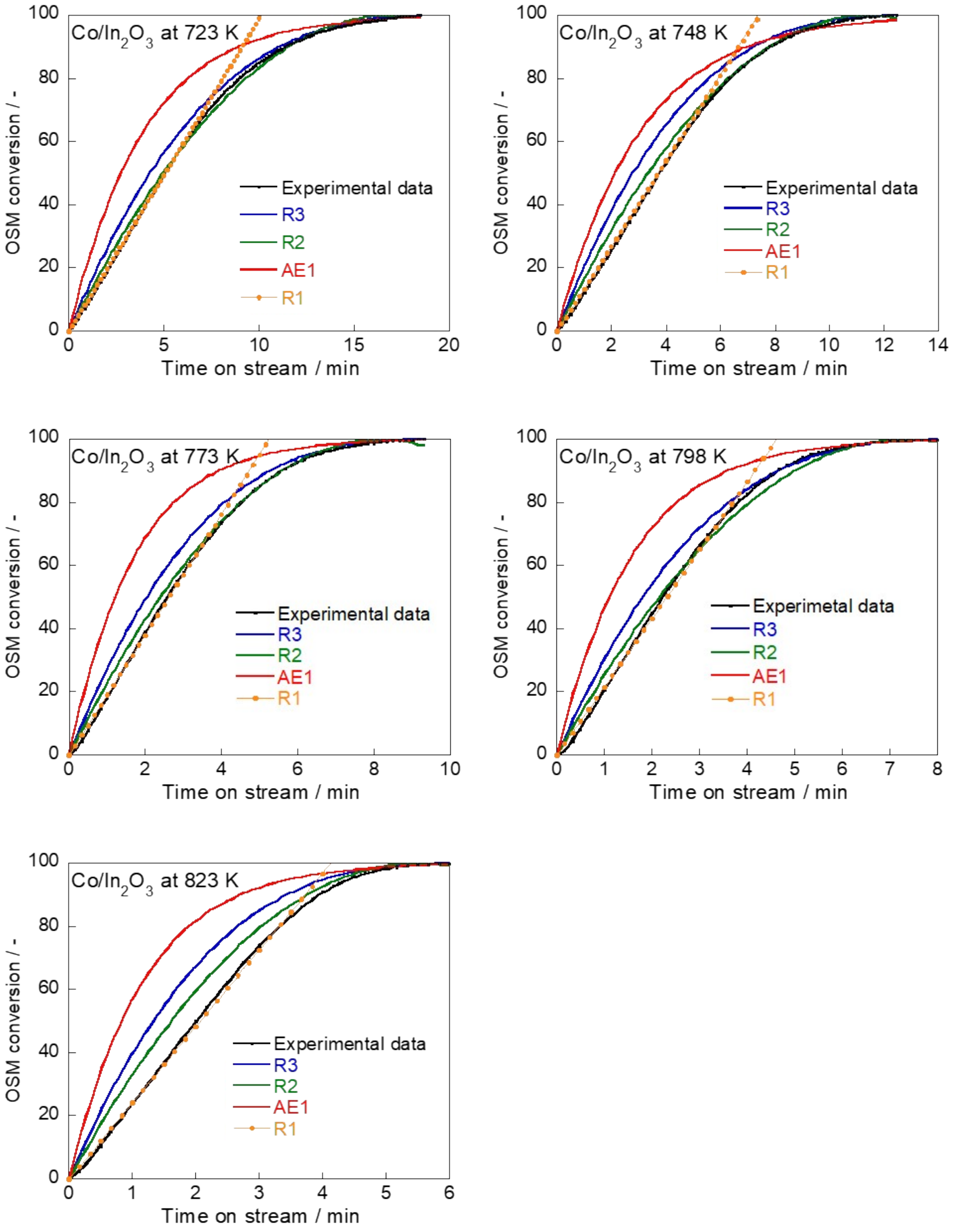

Fig. S5. Comparison of experimental data for oxidation of the reduced Co-In$_2$O$_3$ by CO$_2$ with Avrami-Erofe'ev model (AE1), Zero-order reaction model (R1) and Phase-boundary controlled reaction model (R2 and R3).

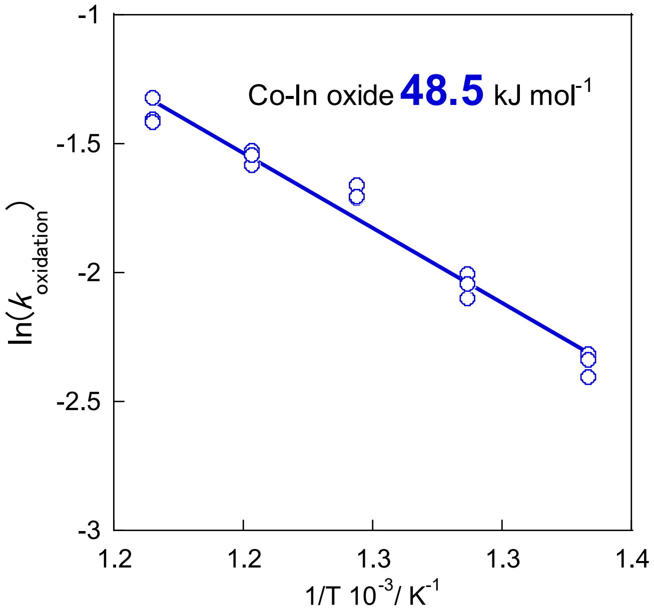

Fig. S6 Arrhenius plot for Co-In_2O_3.

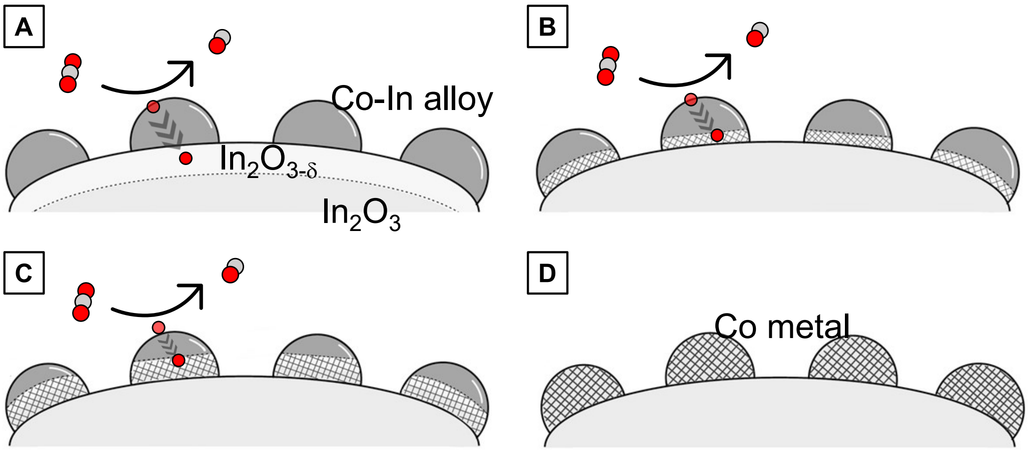

Fig. S7 Oxidation mechanisms of Co-In_2O_3.

Table S1. CO_2 splitting amount, average splitting rate and conversion per cycle in isothermal RWGS-CL test.

Cycle number	CO_2 splitting amount /mmol g^{-1}	Average CO_2 splitting rate /μmol min^{-1} g^{-1}	CO_2 conversion /%
1	2.73	257.8	1.89
2	3.22	293.2	2.15
3	3.20	281.8	2.07
4	3.24	294.0	2.16
5	3.25	293.3	2.15
6	3.27	299.3	2.20
7	3.26	275.5	2.02
8	3.25	282.6	2.07
9	3.23	288.0	2.11
10	3.24	281.8	2.07

Table S2. Ratio of In(0) during the reduction at 773 K, as estimated by linear combination fitting of In *K*-edge spectra.

Reduction time / min	Ratio of In (0) during reduction step / %
10	4.6
20	9.7
30	13.6
40	18.0
50	23.6
60	27.9

Table S3. Rate equations and n values for typical solid-state reaction models.

Function	Reaction model	Equation	n
D1	One-dimensional diffusion	$x^2 = kt$	0.62
D2	Two-dimensional diffusion Valensi equation	$(1-x)\ln(1-x) + x = kt$	0.57
D3	Three-dimensional diffusion Jander equation	$[1-(1-x)^{1/3}]^2 = kt$	0.54
AE1	Avrami-Erofe'ev (n = 1)	$-\ln(1-x) = kt$	1
AE3	Avrami-Erofe'ev (n = 3)	$-\ln(1-x)^{1/3} = kt$	3
R1	Zero order	$x = kt$	1.24
R2	Phase-boundary-controlled reaction (contracting area)	$1-(1-x)^{1/2} = kt$	1.11
R3	Phase-boundary-controlled reaction (contracting volume)	$1-(1-x)^{1/3} = kt$	1.07

Table S4. Values of root-mean square deviation to compare the calculation conversion and the experimental conversion for the oxidation of Co-In_2O_3.

Temperature / K	Root Mean Square Deviation			
	R2 ($x \le 1.0$)	R1 ($x \le 1.0$)	R2 ($x \le 0.7$)	**R1 ($x \le 0.7$)**
723	0.0185	0.3458	0.0246	**0.0087**
	0.0282	0.2802	0.0423	**0.0114**
	0.0337	0.3210	0.0455	**0.0079**
748	0.0340	0.2710	0.0513	**0.0112**
	0.0376	0.2638	0.0564	**0.0224**
	0.0156	0.3361	0.0195	**0.0133**
773	0.0240	0.3174	0.0360	**0.0113**
	0.0244	0.4551	0.0230	**0.0153**
	0.0219	0.4336	0.0211	**0.0166**
798	0.0272	0.3456	0.0343	**0.0172**
	0.0387	0.3314	0.0563	**0.0122**
	0.0287	0.3200	0.0428	**0.0166**
823	0.0569	0.1899	0.0809	**0.0193**
	0.0601	0.2153	0.0864	**0.0140**
	0.0386	0.3518	0.0586	**0.0173**

Table S5. RWGS-CL performance of various Co-In oxides.

OSM	Co/In ratio / -	CO_2 splitting amount /mmol g^{-1}	Average CO_2 splitting rate /μmol min^{-1} g^{-1}
5wt% Co/In_2O_3(a)	0.13	2.55	325
10wt% Co/In_2O_3(a)	0.27	2.58	300
16.5wt% Co/In_2O_3(b)*	0.5	3.25	287

(a)result of RWGS-CL for 5 cycles, (b)result of RWGS-CL for 10 cycles

*Co-In_2O_3 in the main article represents 16.5wt%Co/In_2O_3